



ELSEVIER

Contents lists available at ScienceDirect

## Organic Electronics

journal homepage: [www.elsevier.com/locate/orgel](http://www.elsevier.com/locate/orgel)

## Novel soluble pentacene and anthradithiophene derivatives for organic thin-film transistors

Choongik Kim<sup>a,†</sup>, Peng-Yi Huang<sup>b,†</sup>, Jhe-Wei Jhuang<sup>b</sup>, Ming-Chou Chen<sup>b,\*</sup>, Jia-Chong Ho<sup>c</sup>, Tarnng-Shiang Hu<sup>c</sup>, Jing-Yi Yan<sup>c</sup>, Liang-Hsiang Chen<sup>c</sup>, Gene-Hsiang Lee<sup>d</sup>, Antonio Facchetti<sup>a,\*</sup>, Tobin J. Marks<sup>a,\*</sup>

<sup>a</sup> Department of Chemistry and The Materials Research Center, Northwestern University, 2145 Sheridan Rd., Evanston, IL 60208-3113, USA

<sup>b</sup> Department of Chemistry, National Central University, Jhong-Li 32054, Taiwan, ROC

<sup>c</sup> Industrial Technology Research Institute, Taiwan, ROC

<sup>d</sup> Instrumentation Center, National Taiwan University, Taipei 10660, Taiwan, ROC

## ARTICLE INFO

## Article history:

Received 4 March 2010

Received in revised form 27 April 2010

Accepted 30 April 2010

Available online 13 May 2010

## Keywords:

Organic thin-film transistor

Organic semiconductor

Solution-process

Pentacene

Anthradithiophene

## ABSTRACT

Four new solution-processable pentacene- (**PEN**) and anthradithiophene- (**ADT**) based organic semiconductors bearing two phenylethynyl (**PE-**) or triethylsilylphenylethynyl (**TESPE-**) substituents have been synthesized, characterized, and incorporated in thin-film transistors (TFTs). The molecular structures of these four materials have been determined by single-crystal X-ray diffraction. Thin films of all four compounds have been fabricated via drop-casting and exhibited p-channel OTFT transport with hole mobilities as high as  $\sim 0.01 \text{ cm}^2/\text{V s}$ . Compared to **PEN** derivatives, **ADT**-based compounds exhibited superior device performance and photooxidative stability in ambient. The film morphologies and microstructures of these compounds have been characterized by optical microscopy and X-ray diffraction to rationalize device performance trends.

© 2010 Elsevier B.V. All rights reserved.

### 1. Introduction

Solution-processable organic semiconductors have attracted extensive research attention as components in organic thin-film transistors (OTFTs) for disposable, inexpensive, large-area electronics, such as electronic papers, sensors, and smart textiles [1,2]. Among the well-developed organic semiconductor classes, pentacene (**PEN**) [3], anthradithiophene (**ADT**) [4], and fused-thiophene [5] derivatives are archetypical small-molecule semiconductors. These small molecules are not very soluble in common solvents, which limits their applicability in many high-throughput coating and printing processes. Furthermore, pentacene suffers from oxidative instability

by photooxidation at the C-6/C-13 positions [3]. There have been a number of reports addressing the limitations of small molecule organic semiconductors by pursuing solution-processable compounds with enhanced oxidative stability. Among these efforts, pentacene precursors **A** [6] and pentacene derivatives **B–D** [7] are representative examples. Although these strategies have not yet been fully successful [8], introducing substituents at the pentacene C-6/C-13 positions has proven to be effective at enhancing the stability of the pentacene framework and derivatives with greatly improved carrier mobility has been reported. For example, triisopropylsilylphenylethynyl (TIPS)-substituted pentacene (**TIPS-PEN**; **B**) exhibited enhanced ambient stability [7a], while 4-pentylphenylethynyl-substituted pentacene (**BPPE-PEN**; **C**) showed carrier mobility as high as  $0.52 \text{ cm}^2/\text{V s}$ , attributable to the extended  $\pi$ -electron delocalization between the pentacene core and the substituents [3g]. For **ADT** derivatives, similar approaches have been investigated, and a solution-pro-

\* Corresponding authors. Tel.: +886 34273253; fax: +886 34227664.

E-mail addresses: [mcchen@ncu.edu.tw](mailto:mcchen@ncu.edu.tw) (M.-C. Chen), [a-facchetti@northwestern.edu](mailto:a-facchetti@northwestern.edu) (A. Facchetti), [t-marks@northwestern.edu](mailto:t-marks@northwestern.edu) (T.J. Marks).

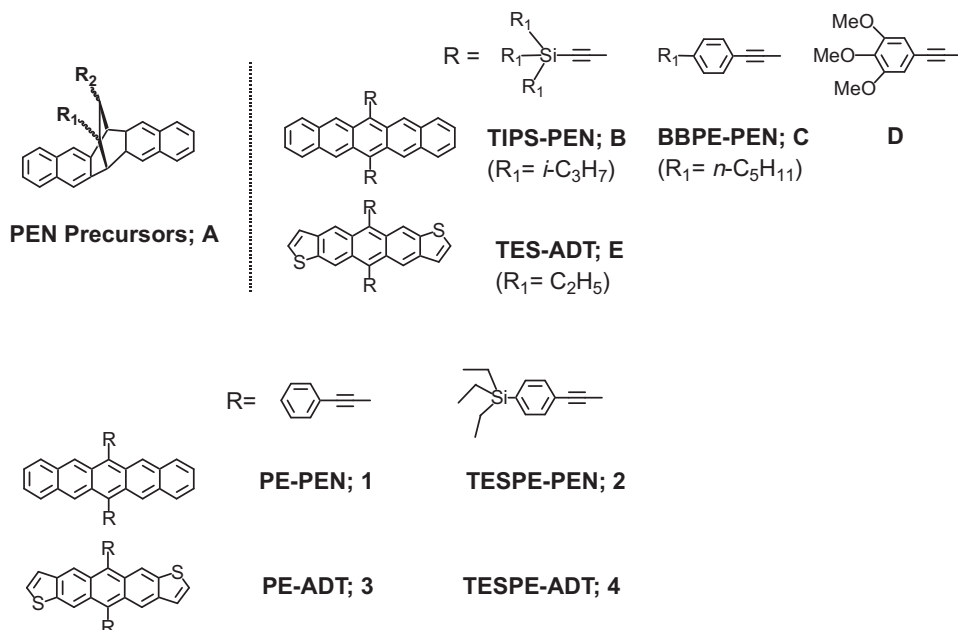
† These authors contributed equally to this work.

cessable p-channel triethylsilylethynyl **ADT** derivative (**TES-ADT**; **E**) with a mobility as high as  $1.0 \text{ cm}^2/\text{Vs}$  was reported by Jackson and co-workers [9]. Meanwhile, trimethoxyphenylethynyl-substituted **PEN** and **ADT** (**D**) derivatives have also been reported with relatively low carrier mobility from solution-processed films [10]. All of these studies demonstrated that ethynyl/phenyl substituents on the **PEN/ADT** cores significantly influence the solid state electrical performance [11]. Presumably, more conjugated phenyl groups connected to the ethynyl group might be expected to further enhance self-assembly of the aromatic moieties into closely  $\pi$ -stacked arrays, therefore improving intermolecular orbital overlap and the resulting device performance. To prove this postulation, four solution-processable **PEN** and **ADT** derivatives (**1–4**) bearing phenylethynyl and triethylsilylphenylethynyl substituents were synthesized, characterized, and incorporated in OTFTs. From the single-crystal X-ray diffractions and film morphologies of these four compounds, it has been clearly seen that both substituents did strongly affect the intermolecular stacking of these new derivatives. With the bulky triethylsilyl (TES) moiety appended to the phenylethynyl group, the molecular packings of compounds **2** and **4** via X-ray analysis were peculiarly engaged in 2-D “slipped-crossed” stacking to accommodate the bulky TES groups, which were very different from those of compounds **1** and **3**, and therefore, substantially directed their electronic performance fabricated via drop-casting (*vide infra*).

## 2. Experimental section

### 2.1. Materials and methods

All chemicals and solvents used in this work were of reagent grade and were obtained from Aldrich, Arco, or TCI Chemical Co. Reaction solvents (toluene, benzene, ether, and THF) were distilled under nitrogen from sodium/benzophenone ketyl, and halogenated solvents were distilled from  $\text{CaH}_2$ .  $^1\text{H}$  and  $^{13}\text{C}$  NMR spectra were recorded on a Bruker 500 or a Bruker DRX-200 instrument. Differential scanning calorimetry (DSC) was carried out on a Mettler DSC 822 instrument at a scan rate of 10 K/min. Thermogravimetric analysis (TGA) was performed on a Perkin-Elmer TGA-7 thermal analysis system using dry nitrogen as a carrier gas at a flow rate of 40 mL/min. The optical absorption and fluorescence spectra were obtained using JASCO V-530 and Hitachi F-4500 spectrometers, respectively, and all spectra were measured in a specified solvent at room temperature. The IR spectra were obtained using a JASCO FT/IR-4100 spectrometer. Differential pulse voltammetry experiments were performed using a CH Instruments/CHI621C Electrochemical Analyzer. All measurements were carried out at the temperatures indicated with a conventional three-electrode configuration consisting of a platinum disk working electrode, an auxiliary platinum wire electrode, and a non-aqueous Ag reference electrode. The supporting electrolyte was 0.1 M tetrabutylammonium hexafluorophosphate ( $\text{TBAPF}_6$ ) in a specified dry solvent. All potentials reported were referenced to an  $\text{Fc}^+/\text{Fc}$  internal



standard (at +0.6 V). Elemental analyses were performed on a Heraeus CHN-O-Rapid elemental analyzer. Mass spectrometric data were obtained with a JMS-700 HRMS instrument. Prime grade silicon wafers (p<sup>+</sup>-Si) with ~300 nm (±5%) of thermally grown oxide (from Montco Silicon) were used as device substrates.

## 2.2. Synthesis

### 2.2.1. Synthesis of 6,13-bis(phenylethynyl)pentacene (**PE-PEN**; **1**)

The procedure was reported in the literature [12]. <sup>1</sup>H NMR (200 MHz, CDCl<sub>3</sub>): δ 9.32(s, 4H), 8.08(dd, *J* = 6 Hz, 3 Hz, 4H), 7.93(dd, *J* = 8 Hz, 1 Hz, 4H), 7.55–7.41(m, 10H). Deep blue crystals suitable for X-ray diffraction were crystallized by slow diffusion of hexane into a xylene solution of compound **1**. The molecular structure of **1** was confirmed by X-ray diffraction and is shown in Fig. 4 below (cif file of **1** is in SI).

### 2.2.2. Synthesis of 4-triethylsilylphenyl acetylene (**5**) [13]

As shown in Scheme 1, under nitrogen, 35.6 mL of 2.5 M *n*-BuLi (in hexane, 0.089 mol) was slowly added to a 100 mL dry ether solution of 1,4-dibromobenzene (20 g, 0.085 mol) at –50 to –30 °C, and the mixture was then stirred at 0 °C for 1 h. Next, 15.1 mL of chlorotriethylsilane (0.085 mol) was slowly added to the above mixture and stirring was continued for 8 h. Water was then added to the reaction mixture, and the organic layer was collected. After solvent evaporation, the desired oily 1-bromo-4-triethylsilylbenzene was purified by distillation at 110 °C/0.02 Torr giving 21.7 g of product (94% yield). <sup>1</sup>H NMR (CDCl<sub>3</sub>): δ 7.47(d, *J* = 8 Hz, 2H), 7.33(d, *J* = 8 Hz, 2H), 0.96(t, *J* = 8 Hz, 9H), 0.78(q, *J* = 8 Hz, 6H).

Under nitrogen, a mixture of dry 1-bromo-4-triethylsilylbenzene (2.0 g, 7.4 mmol), Pd(PPh<sub>3</sub>)<sub>2</sub>Cl<sub>2</sub> (0.103 g, 0.15 mmol), CuI (56 mg, 0.3 mmol), and 15 mL of dry piperidine was stirred at 0 °C for 10 min, and then trimethylsilylacetylene (1.58 mL, 11 mmol) was added to the mixture. The mixture was then stirred at 80 °C for 18 h. After cooling to room temperature, the solvent was removed under vacuum, and a methanol (20 mL) solution of K<sub>2</sub>CO<sub>3</sub> (3.07 g, 22.2 mmol) was added to the mixture and stirring was continued at room temperature for 2 h. The methanol was then removed under vacuum, and the organic product was extracted with hexane and then filtered through a Celite flash column. The concentrated crude product was fi-

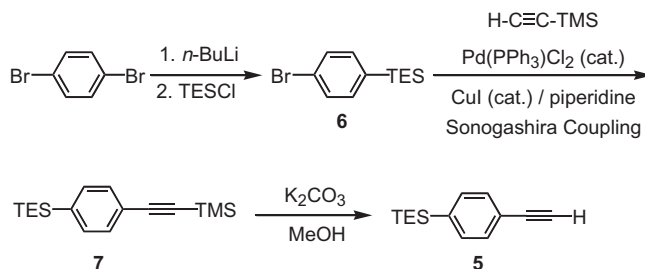
nally purified via chromatography (silica gel; hexane as the eluent) giving 1.36 g of desired oily product (85% yield). <sup>1</sup>H NMR(CDCl<sub>3</sub>): δ 7.46–7.45(m, 4H), 3.09(s, 1H, C-H), 0.95(t, *J* = 8 Hz, 9H), 0.79(q, *J* = 8 Hz, 6H).

### 2.2.3. Synthesis of 6,13-(4-triethylsilylphenylethynyl)-pentacene (**TESPE-PEN**; **2**)

Under nitrogen, 2.5 mL of 2.5 M *n*-BuLi (in hexane, 6.25 mmol) was slowly added to a 20 mL THF solution of 4-triethylsilylphenylacetylene (1.24 g, 5.7 mmol) at 0 °C, and the mixture was stirred at 60 °C for 3 h. The resulting black-brown lithium phenyl acetylide solution was then transferred to a dry THF (50 mL) solution of pentacene-6,13-dione (0.3 g, 1.0 mmol) at 0 °C, and the mixture was refluxed for 12 h. After cooling to room temperature, 5 mL of water was added into the reaction mixture and a deoxygenated SnCl<sub>2</sub> (3 g, 15.7 mmol)/HCl (5 mL, 10%) solution was added to the reaction and stirring was continued at room temperature for 3 h. Water was added to the reaction mixture and the organic layer was collected and purified by chromatography (silica gel; hexanes as the eluent) and recrystallization from hexane, giving 39 mg of blue solid (5.6% yield). <sup>1</sup>H NMR (200 MHz, CDCl<sub>3</sub>): δ 9.29(s, 4H), 8.04(m, 4H), 7.87(d, *J* = 8 Hz, 4H), 7.65(d, *J* = 8 Hz, 4H), 7.41(m, 4H), 0.91(t, *J* = 8.0 Hz, 18H), 0.85(q, *J* = 8.0 Hz, 12H). Deep green crystals suitable for X-ray diffraction were crystallized by slow evaporation of an ether solution of compound **2**. The molecular structure of **2** was confirmed by X-ray diffraction and is shown in Fig. 6 below (cif file of **2** is in SI).

### 2.2.4. Synthesis of 5,11-bis(phenylethynyl)anthradithiophene (**PE-ADT**; **3**)

Under nitrogen, 7.6 mL of 2.5 M *n*-BuLi (in hexane, 0.019 mol) was slowly added to a 20 mL dioxane solution of phenylacetylene (1.95 g, 0.019 mol) at 0 °C, and the mixture was stirred at room temperature for 1 h. The resulting black-brown solution was transferred to a dry dioxane solution (30 mL) of anthradithiophene-5,11-dione [4a] (0.306 g, 0.96 mmol) at 0 °C, and then the mixture was refluxed for 4 h. After cooling to room temperature, 0.5 M NH<sub>4</sub>Cl solution (50 mL, 0.25 mol) was added to the reaction mixture, and the organic layer was collected. Hexane was then added to the collected solution to precipitate green-brown 5,11-dihydroxy-5,11-bis(phenylethynyl) anthradithiophene (0.28 g, 54% yield). <sup>1</sup>H NMR (200 MHz, CDCl<sub>3</sub>):



**Scheme 1.** Synthesis of 4-triethylsilylphenyl acetylene **5**.

$\delta$  8.79(s, 2H), 8.73(s, 2H), 7.76–7.72(m, 4H), 7.56(d,  $J = 5$  Hz, 2H), 7.47–7.35(m, 8H), 4.33(t,  $J = 5$  Hz, 2H, OH).

Under nitrogen, a deoxygenated acetic acid (7.5 mL, 50%) solution of SnCl<sub>2</sub> (8.4 g, 0.044 mol) was added to the above dioxane solution (45 mL) of 5,11-dihydroxyl-5,11-bis(phenylethynyl)anthradithiophene (0.28 g, 0.53 mmol), and the mixture was stirred at room temperature for 2 h. Next, water was added to the resulting pink-red solution and the resulting purple precipitate was collected by filtration and washed with ether and hexane. The product was further purified via recrystallization from *p*-xylene giving 0.12 g of the product (46% yield). <sup>1</sup>H NMR (200 MHz, CDCl<sub>3</sub>):  $\delta$  9.23(s, 2H), 9.17(s, 2H), 7.87–7.84(m, 4H), 7.57–7.47(m, 10H). MS (FAB) ( $m/z$ ) calcd. for C<sub>34</sub>H<sub>18</sub>S<sub>2</sub>: 490 (M<sup>+</sup>), Found: 490. Purple-red crystals suitable for X-ray diffraction were crystallized by slow diffusion of hexane into a xylene solution of compound **3**. The molecular structure of **3** was confirmed by X-ray diffraction and is shown in Fig. 5 below (cif file of **3** is in SI).

### 2.2.5. Synthesis of 5,11-Bis(4-triethylsilylphenylethynyl)-anthradithiophene (TESPE-ADT; **4**)

Under nitrogen, 2.0 mL of 2.0 M isopropyl magnesium chloride (4.0 mmol) in THF was slowly added to a 20 mL THF solution of 4-triethylsilylphenylacetylene (0.86 g, 3.95 mmol) at 0 °C, and the mixture was stirred at 60 °C for 2 h. The resulting black-brown solution was then transferred to a dry THF solution (50 mL) of an anthradithiophene-5,11-dione (200 mg, 0.624 mmol) at room temperature, and then the mixture was refluxed at 60 °C overnight. After cooling to room temperature, 1.5 mL of water and a deoxygenated SnCl<sub>2</sub> (3.0 g, 15.7 mmol)/HCl

(5 mL, 10%) solution was added to the reaction mixture, and stirring was continued at 60 °C for 3 h. Water was next added to the reaction mixture, and the organic layer was collected and purified by chromatography (silica gel; hexane as the eluent) and recrystallization from ether, giving 160 mg of purple-red precipitate (36% yield). <sup>1</sup>H NMR (300 MHz, CDCl<sub>3</sub>):  $\delta$  9.22(s, 2H), 9.16(s, 2H), 7.83(d,  $J = 7.5$  Hz, 4H), 7.63(d,  $J = 7.5$  Hz, 4H), 7.56(d,  $J = 6$  Hz, 2H), 7.48(d,  $J = 6$  Hz, 2H), 1.02(t,  $J = 7.5$  Hz, 18H), 0.88(t,  $J = 7.5$  Hz, 12H). Purple-red crystals suitable for X-ray diffraction were crystallized by slow evaporation of an ether solution of compound **4**. The molecular structure of **4** was confirmed by X-ray diffraction and is shown in Fig. 7 below (cif file of **4** is in SI).

### 2.3. X-ray crystal structure determinations of compounds 1–4

The selected crystals were mounted on a glass fiber. Data collection on compounds **1–3** and **4** were carried out on a BRUKER SMART APEX CCD and a NONIUS Kappa CCD diffractometer, respectively, with Mo radiation ( $\lambda = 0.71073$  Å) at 150(2) K. After data collection, the frames were integrated and absorption corrections were applied. The initial crystal structure was solved by a direct method, the structure solution was expanded through successive least-squares cycles, and the final solution was determined. All non-hydrogen atoms were refined anisotropically. Hydrogen atoms attached to the carbons were fixed at calculated positions and were refined using a riding mode. Crystal data, data collection, and refinement parameters are summarized in Table 1.

**Table 1**

Summary of crystal structure data for compounds **1–4**.<sup>a</sup>

Compound	<b>1</b>	<b>2</b>	<b>3</b>	<b>4</b>
Empirical formula	C <sub>38</sub> H <sub>22</sub>	C <sub>50</sub> H <sub>50</sub> Si <sub>2</sub>	C <sub>34</sub> H <sub>18</sub> S <sub>2</sub>	C <sub>46</sub> H <sub>46</sub> S <sub>2</sub> Si <sub>2</sub>
Formula weight	478.56	707.08	490.60	719.13
Temperature (K) <sup>b</sup>	150(2)	150(2)	150(2)	150(2)
Crystal system	Triclinic	Orthorhombic	Monoclinic	Triclinic
Space group	<i>P</i> $\bar{1}$	<i>Pca</i> 2(1)	<i>P</i> 2(1)/ <i>n</i>	<i>P</i> $\bar{1}$
Unit cell dimensions (Å)	<i>a</i> = 10.1371(6) $\alpha$ = 72.515(1)° <i>b</i> = 12.9940(7) $\beta$ = 82.654(1)° <i>c</i> = 19.8189(11) $\gamma$ = 78.759(1)°	<i>a</i> = 23.6356(11) $\alpha$ = 90° <i>b</i> = 47.245(2) $\beta$ = 90° <i>c</i> = 7.3483(3) $\gamma$ = 90°	<i>a</i> = 12.019(3) $\alpha$ = 90° <i>b</i> = 5.3975(11) $\beta$ = 100.571(5)° <i>c</i> = 18.780(4) $\gamma$ = 90°	<i>a</i> = 7.4170(3) $\alpha$ = 81.015(2)° <i>b</i> = 12.5298(6) $\beta$ = 85.000(2)° <i>c</i> = 22.1051(10) $\gamma$ = 85.107(2)°
<i>V</i> (Å <sup>3</sup> )	2435.5(2)	8205.5(6)	1197.6(4)	2016.01(16)
<i>Z</i>	4	8	2	2
<i>d</i> (calc) (g/cm <sup>3</sup> )	1.305	1.145	1.361	1.185
Absorption coefficient (mm <sup>-1</sup> )	0.074	0.120	0.245	0.222
<i>F</i> (0 0 0)	1000	3024	508	764
Crystal size (mm)	0.70 × 0.10 × 0.07	0.70 × 0.10 × 0.10	0.70 × 0.07 × 0.01	0.60 × 0.10 × 0.10
Reflections collected	26,841	70,259	5790	17,924
Independent reflections	8571	14,375	2113	7008
<i>R</i> <sub>int</sub>	0.0536	0.0940	0.1229	0.0544
Final <i>R</i> indices [ <i>I</i> > 2σ( <i>I</i> )] <sup>c</sup>	<i>R</i> <sub>1</sub> = 0.0961 <i>wR</i> <sub>2</sub> = 0.2501	<i>R</i> <sub>1</sub> = 0.0809 <i>wR</i> <sub>2</sub> = 0.1580	<i>R</i> <sub>1</sub> = 0.1674 <i>wR</i> <sub>2</sub> = 0.3203	<i>R</i> <sub>1</sub> = 0.0636 <i>wR</i> <sub>2</sub> = 0.1727
<i>R</i> indices (all data)	<i>R</i> <sub>1</sub> = 0.1489 <i>wR</i> <sub>2</sub> = 0.2883	<i>R</i> <sub>1</sub> = 0.1019 <i>wR</i> <sub>2</sub> = 0.1694	<i>R</i> <sub>1</sub> = 0.2107 <i>wR</i> <sub>2</sub> = 0.3432	<i>R</i> <sub>1</sub> = 0.1014 <i>wR</i> <sub>2</sub> = 0.1949

<sup>a</sup> CCD area detector diffractometer; Mo K $\alpha$  radiation;  $\lambda = 0.71073$  Å.

<sup>b</sup> Temperature for data collection.

<sup>c</sup> Refinement method: full-matrix least-squares on *F*<sup>2</sup>.

## 2.4. Semiconductor film deposition and characterization

All p<sup>+</sup>-Si/SiO<sub>2</sub> substrates were cleaned via sonication in absolute ethanol for 3 min and then by oxygen plasma treatment for 5 min (20 W, 0.5 Torr). For an SiO<sub>2</sub> coating layer, -SiMe<sub>3</sub> groups were introduced using hexamethyldisilazane (HMDS) and were deposited by placing the clean SiO<sub>2</sub> substrates in a N<sub>2</sub>-filled chamber saturated with HMDS vapor for 48–72 h. For vacuum deposition, semiconducting materials were thermally deposited at  $\sim 6 \times 10^{-6}$  Torr ( $\sim 500$  Å, 0.2–0.3 Å/s) at 20 or 50 °C. For drop-casting, a 0.1–0.2 wt.% solution (in toluene, tetrachloromethane, chlorobenzene, or dichlorobenzene) of each compound was placed on a clean substrate (1 cm × 1 cm) on a hot plate at a preset temperature. The temperature setting was  $\sim 50$  °C lower than the boiling point of the corresponding solvent. The substrates were kept under a saturated vapor of solvent (the same solvent used to dissolve the compound) until the solvent evaporated completely. Films were then annealed in a vacuum oven to remove the residual solvent. Thin films of the organic semiconductors were analyzed by optical microscopy and wide angle  $\theta - 2\theta$  X-ray diffraction (XRD) (Rigaku ATXG) using monochromated Cu K $\alpha$  radiation. For TFT device fabrication, top-contact electrodes ( $\sim 70$  nm) were deposited by evaporating gold ( $\sim 1 \times 10^{-6}$  Torr) through a shadow mask with a channel length (*L*) of 100  $\mu$ m and a channel width (*W*) of 500–5000  $\mu$ m.

## 2.5. Electrical Measurements

All OTFT measurements were carried out in ambient conditions using a Keithly 6430 subfemtoammeter and a Keithly 2400 source meter, operated by a local Labview program and GPIB communication. The mobilities ( $\mu$ ) were calculated in the saturation regime using the relationship [14]:  $\mu_{\text{sat}} = (2I_{\text{DS}}L) / [WC_i(V_G - V_T)^2]$ , where  $I_{\text{DS}}$  is the source–drain saturation current,  $C_i$  is the gate dielectric capacitance (per area),  $V_G$  is the gate voltage, and  $V_T$  is the threshold voltage. The latter can be estimated as the *x* intercept of the linear section of the plot of  $V_G$  vs.  $(I_{\text{DS}})^{1/2}$ .

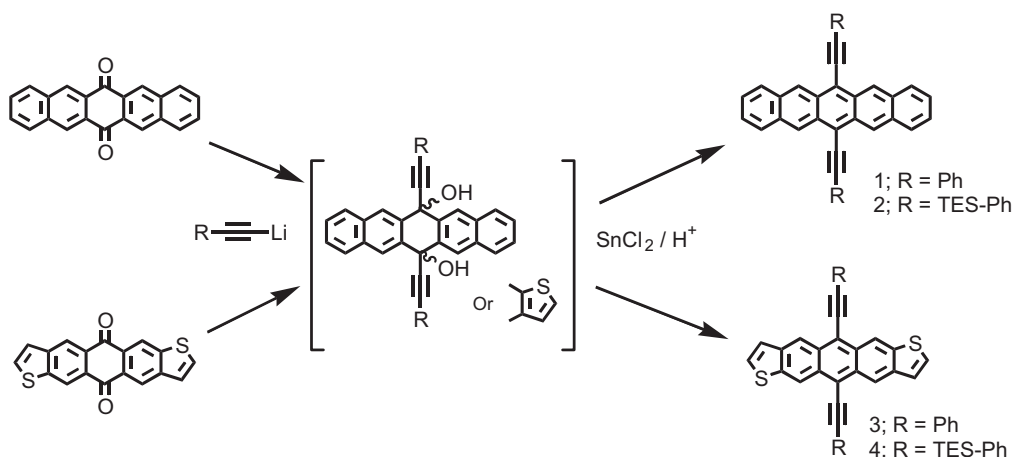
## 3. Results and discussion

### 3.1. Synthesis

The synthesis of four soluble **PEN-** (**1** and **2**) and **ADT-** (**3** and **4**) based compounds was achieved according to **Scheme 2** following known synthetic approaches for other soluble **PEN** or **ADT** derivatives [9]. Starting from pentacene or ADT quinone, phenylethynyl-substituted **1** and **2** as well as triethylsilylphenylethynyl-substituted **3** and **4** were obtained via phenylethynyl anion alkylation and SnCl<sub>2</sub>/HCl reduction, with overall yields of 50%, 6%, 46%, and 36%, respectively. Compared to **PEN** or **ADT**, compounds **1–4** exhibited significantly enhanced solubility in common organic solvents. Noteworthy is that triethylsilylphenylethynyl (**TESPE-**) substituted compounds **2** and **4** were very soluble in common organic solvents such as hexanes, ether, and benzene.

### 3.2. Thermal and optical properties

As summarized in **Table 2**, **ADT** derivatives exhibited greater thermal stability than do the analogous **PEN** derivatives. Thus, compounds **3** and **4** exhibited higher thermal decomposition temperatures (339 and 168 °C, respectively) than compounds **1** and **2** (255 and 86 °C, respectively). Note that **ADT** derivative **3**, the most thermally stable compound prepared in this study, did not exhibit a melting endotherm up to 339 °C in differential scanning calorimetry (DSC) measurements and exhibited weight loss only on heating above 320 °C, as demonstrated by thermogravimetric analysis. Compared to the phenylethynyl groups, triethylsilylphenylethynyl substituents significantly decreased the thermal stability of the corresponding arenes. In particular, pentacene derivative **2** decomposed at 86 °C, which might explain the low synthetic yield of the corresponding compound. **Pen** and **ADT** derivatives with the present core substituents exhibited significantly red-shifted optical absorption spectra. Pentacene derivatives **1** and **2** in C<sub>6</sub>H<sub>5</sub>Cl exhibited  $\lambda_{\text{max}}$  values of  $\sim 664$  nm (vs.  $\sim 579$  nm for pentacene), while **ADT**



**Scheme 2.** Synthesis of soluble **PEN** and **ADT** derivatives **1–4**.

**Table 2**  
Thermal, optical absorption/emission, and electrochemical data for compounds **1–4**.

Comp.	Decomp. $T_d$ (°C)	TGA (°C; 5%)	Optical <sup>b</sup> $\lambda_{\max}$ (nm)	Reductive potential (V) <sup>c</sup>	Oxidative potential (V) <sup>c</sup>	$\Delta E_{\text{gap}}$ (eV)	
						(UV) <sup>b</sup>	(DPV) <sup>c</sup>
<b>1</b>	255	423	662	−0.924	0.876	1.76	1.80
<b>2</b>	86	382	666	−0.864	0.836	1.73	1.70
<b>PEN</b>	373 <sup>a</sup>	297	579	−1.27	0.820	2.07	2.09
<b>3</b>	339	320	571	−1.14	0.948	2.06	2.09
<b>4</b>	168	239	576	−1.14	0.956	2.05	2.10
<b>ADT</b>	450 <sup>a</sup>	306	490	−1.63	0.940	2.47	2.57

<sup>a</sup> Melting temperature.

<sup>b</sup> In  $\text{C}_6\text{H}_5\text{Cl}$ .

<sup>c</sup> In  $o\text{-C}_6\text{H}_4\text{Cl}_2$  at 100 °C ( $\text{Fc}/\text{Fc}^+$  as an internal standard at +0.6 V).

derivatives **3** and **4** exhibited  $\lambda_{\max}$  values of  $\sim 574$  nm (vs.  $\sim 490$  nm for ADT; Fig. 1), demonstrating extended  $\pi$ -electron delocalization from the molecular core to the phenylethenyl substituents. Calculated from the onset of the optical absorption, pentacene derivatives **1** and **2** exhibited smaller HOMO–LUMO energy gaps than do ADTs **3** and **4**,

which was consistent with the energy gap values derived electrochemically (*vide infra*).

The photooxidative stability of derivatives **1–4** was investigated by monitoring the absorbance decay at  $\lambda_{\max}$  in aerated  $\text{C}_6\text{H}_5\text{Cl}$  solutions while exposing to white light (fluorescent lamp) at room temperature (Fig. 2) [15].

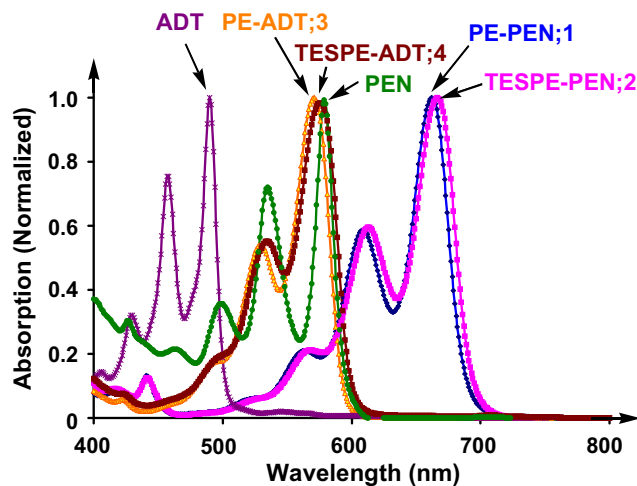


Fig. 1. Optical absorption spectra of compounds **1–4** in  $\text{C}_6\text{H}_5\text{Cl}$  solution.

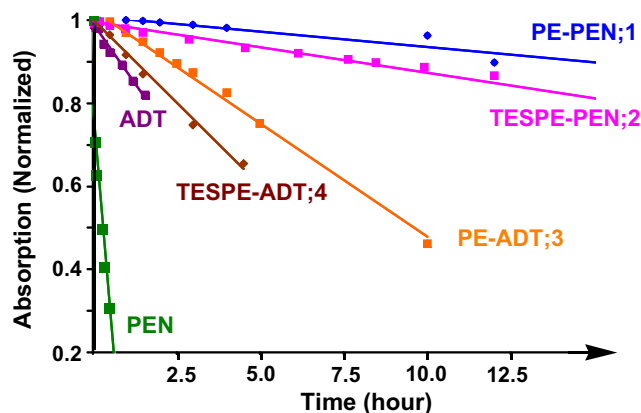


Fig. 2. Photostability of compounds **1–4** in a  $\text{C}_6\text{H}_5\text{Cl}$  solution, as monitored by optical spectroscopy under white light at room temperature.

Decomposition was observed for all compounds under these conditions over 24 h. Nevertheless, the core-substituted compounds in this study exhibited longer half-lives than non-substituted **PEN** and **ADT**, demonstrating enhanced stability via core substitution, as observed for other pentacene derivatives [16]. The phenylethynyl-substituted compounds (**1** and **3**) exhibited enhanced photostability compared to triethylsilylphenylethynyl-substituted derivative **2** and **4**. Note that under ambient conditions ( $O_2$  and  $H_2O$  present) without white light, no decomposition was observed for these soluble **ADTs** and **PENs**, demonstrating their potential as solution-processable organic semiconductors.

### 3.3. Electrochemical characterization

Differential pulse voltammograms (DPVs; using ferrocene/ferrocenium as internal standard at +0.6 V) of compounds **1–4** were recorded in dichlorobenzene at 100 °C [17], and the resulting oxidation and reduction potentials are summarized in Table 2 [18]. For the **PEN** series, the DPV spectra of compounds **1** and **2** exhibited oxidative peaks at +0.84 V and +0.88 V as well as reductive peaks at –0.86 V and –0.92 V, respectively (using ferrocene/ferrocenium as the internal standard at +0.6 V); both oxidative and reductive peaks were shifted to more positive

values than those of **PEN** (+0.82 V and –1.27 V, respectively). Similar shifts of both oxidative and reductive peaks were observed for the **ADT** series. The HOMO levels of the **ADT** derivatives were therefore slightly lower than those of the pentacene derivatives (Fig. 3; assuming ferrocene/ferrocenium oxidation at 4.8 eV). In contrast, the LUMO levels of these soluble compounds were significantly lower in both series compared to unsubstituted **PEN** and **ADT**, which can be attributed to more extensive  $\pi$ -electron delocalization [19]. Overall, the electrochemically-derived HOMO–LUMO energy gaps were ranked in the order of  $1 \approx 2 < \text{PEN} \approx 3 \approx 4 < \text{ADT}$  (Fig. 3), in agreement with the values obtained from optical spectroscopy (Table 2).

### 3.4. Single-crystal structure analysis

The diffraction-derived crystal structures of compounds **1–4** are shown in Figs. 4–7, respectively, and the corresponding data are summarized in Table 1. The molecular packings of phenylethynyl-substituted compounds **1** and **3** were similar to that reported for **BBPE–PEN** [3g]. As shown in Figs. 4–7, the phenyl moieties attached to the ethynyl group were not coplanar with the central **PEN** or **ADT** cores, but had torsional angles of 11.8° and 22.5° (**1**; Fig. 4D), 10.1° (**3**; Fig. 5D), 16.6° (**2**; Fig. 6D), and 18.1° and 28.2° (**4**; Fig. 7D), respectively [20]. The molecular pac-

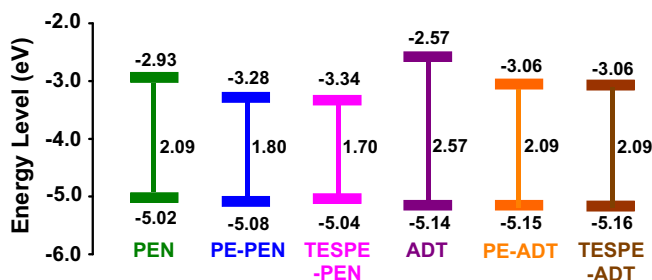


Fig. 3. Electrochemically-derived HOMO and LUMO energies of compounds **1–4**, **PEN**, and **ADT**.

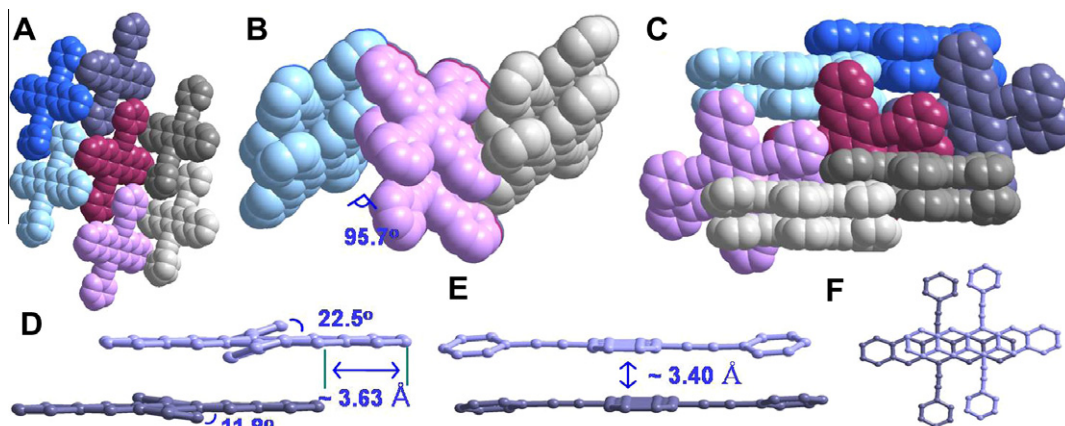
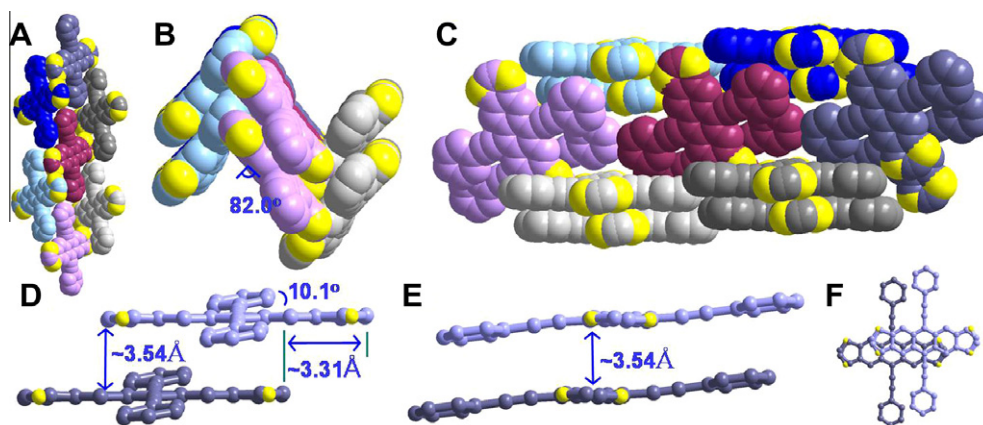


Fig. 4. Crystal structure of compound **1**. (A) Top view (space filling model). (B) Front view. Each of the  $\pi$ -stacks interweave with each other in a herringbone packing at an angle of 95.7°. (C) Side view. (D) Front view. The core interlayer spacing ( $\sim 3.40$  Å) and  $C_6H_5$  groups have torsional angles of about 11.8° and 22.5° with respect to the **PEN** plane. (E) Side view. (F) Top view. The **PEN** cores form 2-D slipped stacks.



**Fig. 5.** Crystal structure of compound **3**. (A) Top view (space filling model). (B) Front view. Each of the **ADT**  $\pi$ -stacks interweave with each other in a herringbone motif at an angle of  $82^\circ$ . (C) Side view. (D) Front view. The core interlayer spacing ( $\sim 3.54$  Å) and  $C_6H_5$  groups have torsional angles of about  $10.1^\circ$  with respect to the **ADT** plane. (E) Side view. (F) Top view. The **ADT** cores form 2-D slipped stacks.

kings of **1** and **3** were similar, exhibiting a herringbone-type packing with tilt angles of  $95.7^\circ$  and  $82.0^\circ$  (Figs. 4B and 5B), respectively [20]. In each packing column, the

**PEN** or **ADT** cores formed 2-D slipped stacks and adopted a nearly face-to-face packing motif (Figs. 4 and 5), with an interplanar angle of  $\sim 0^\circ$  and interplanar distances of

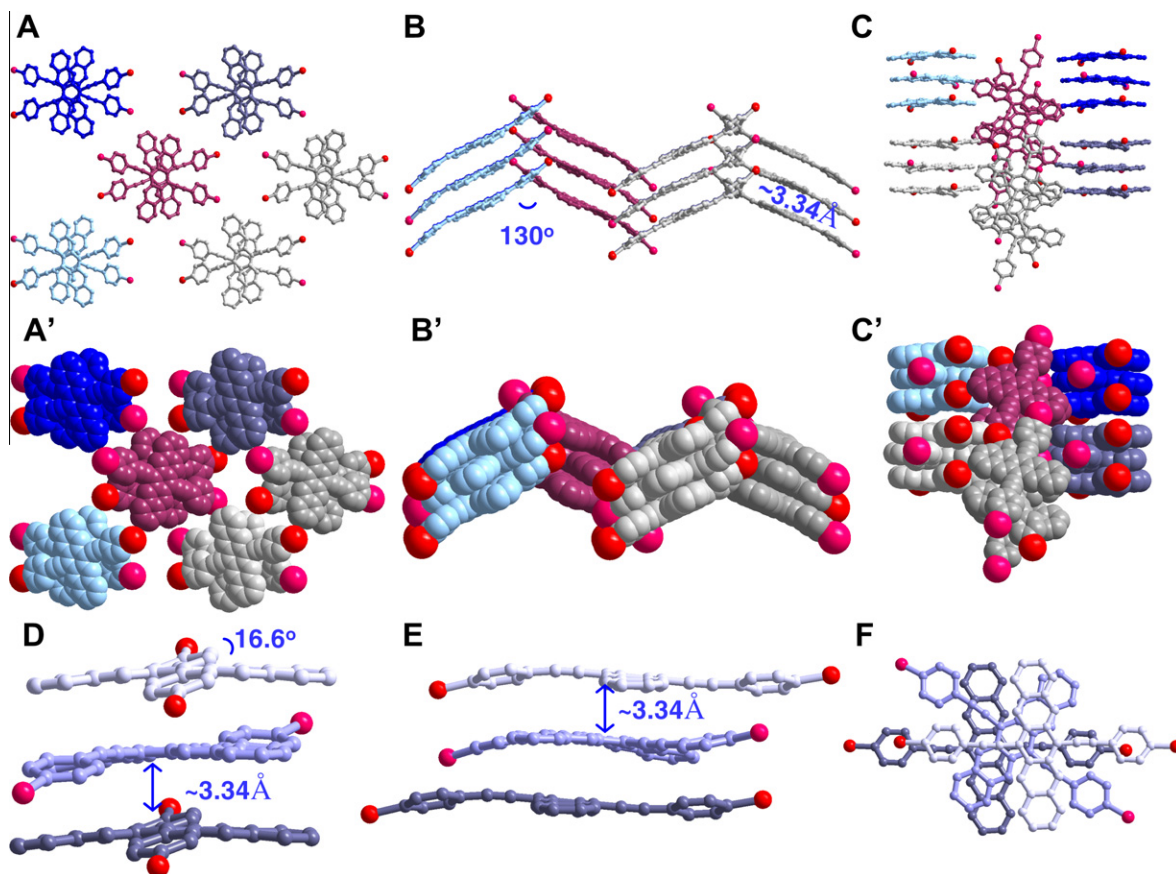


**Fig. 6.** Crystal structure of compound **2**. (A) Top view. The **PEN** cores form 2-D "slipped-crossed" stacks. (B) Front view. Each of the **PEN**  $\pi$ -stacks interweave with one another in a herringbone motif at an angle of  $130^\circ$ . (C) Side view. (D) Front view. The core interlayer separation ( $\sim 3.34$  Å) and the  $C_6H_5$  groups have torsional angles of  $\sim 16.6^\circ$  with respect to the **PEN** plane. (E) Side view. (F) Top view. The "slipped-crossed"  $\pi$ -stacks of **PENs** (A', B', and C' are space filling models of A, B, and C, respectively).

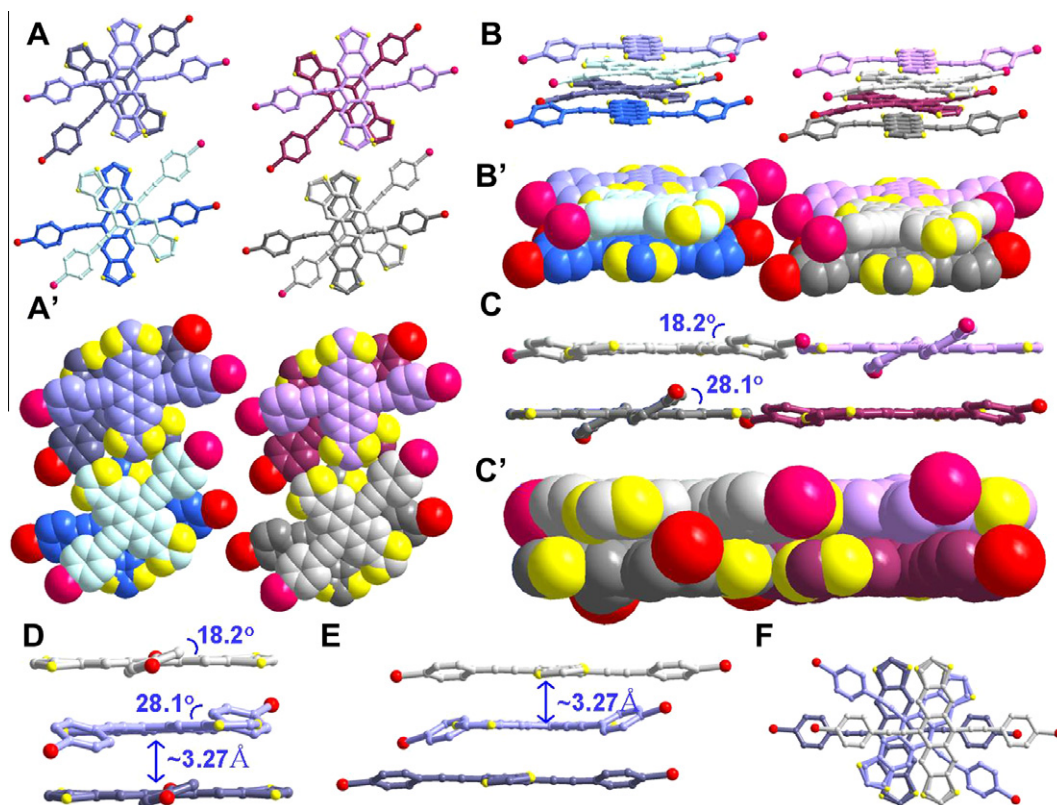


**Fig. 7.** Crystal structure packing of compound **4**. (A) Top view. The ADT cores form 2-D “slipped-crossed” stacks. (B) Front view. Each of the ADT  $\pi$ -stacks interweave with each another. (C) Side view. (D) Front view. The core interlayer separation ( $\sim 3.27$  Å) and  $C_6H_5$  groups have torsional angles of  $\sim 18^\circ$  and  $28^\circ$  with respect to the ADT core. (E) Side view. (F) Top view. The “slipped-crossed”  $\pi$ -stacks of ADTs (A', B', and C' are space filling models of A, B, and C, respectively).

$\sim 3.40$  Å and  $\sim 3.54$  Å (Figs. 4D and 5D), respectively [20]. Note that the PEN or ADT cores were not perfectly aligned with each other but were slipped  $\sim 3.63$  Å (**1**) and  $\sim 3.31$  Å (**3**) along the long axis as well as half a unit cell length along the short axis (Figs. 4E and 5F), revealing a close-packed layered structure with intimate  $\pi$ - $\pi$  overlap.

With the bulky triethylsilyl (TES) moiety appended to the phenylethynyl group, the molecular packings of compounds **2** and **4** were very different from compounds **1** and **3**, as shown in Figs. 6 and 7, respectively. The substitutions of relatively bulky TESPE groups into perpositions of polyacenes did disrupt the herringbone structure of the main Pen and ADT core [21]. Compounds **2** and **4** engaged in 2-D “slipped-crossed” stacking to accommodate the bulky TES groups. For compound **2**, each of the PEN  $\pi$ -stacks interweaved with one another in a herringbone motif at an angle of  $130^\circ$  (Fig. 6B), while this interweaving angle is nearly  $180^\circ$  for compound **4** (Fig. 7B and C). The PEN or ADT cores stacked with interplanar separations of  $\sim 3.34$  Å and  $\sim 3.27$  Å (Figs. 6E and 7E), respectively. Note that this bulky TES substituent induced significant deviations from planarity in the PEN core of compound **2**, in contrast to the other three compounds of this study (Fig. 6D and E). For compound **4**, the interplanar distance is very comparable to those in TES-ADT (3.25 Å) [3a]. The shortest interplanar distance and planarity (with core

interweaving angle of  $\sim 180^\circ$ ) of compound **4** may explain the highest electronic performance among all compounds employed in this study (*vide infra*; [22]).

### 3.5. Thin-film transistor characterization

Top-contact/bottom-gate OTFTs were fabricated by drop-casting [23] films of compounds **1–4** onto bare and HMDS-treated  $p^+$ -Si/SiO<sub>2</sub> substrates (compound **3** was also fabricated via vacuum deposition on both substrates) [24], followed by Au deposition through a shadow mask to define the source and drain electrodes. OTFT characterization

**Table 3**  
Charge carrier mobility ( $\mu$ , cm<sup>2</sup>/V s)<sup>a</sup>, current on/off ratio ( $I_{on}:I_{off}$ ), and threshold voltage ( $V_T$ , V) data for OTFTs fabricated with compounds **1–4** on bare Si/SiO<sub>2</sub> substrates.

Compound	Solvent	$\mu$	$I_{on}:I_{off}$	$V_T$
<b>1</b>	C <sub>6</sub> H <sub>5</sub> Cl	0.001	10 <sup>4</sup>	-1.0
<b>2</b>	C <sub>6</sub> H <sub>5</sub> Cl	0.0004	10 <sup>4</sup>	-7.3
<b>3</b>	C <sub>6</sub> H <sub>5</sub> Cl	0.005	10 <sup>4</sup>	-10.0
<b>3</b> <sup>b</sup>		0.015	10 <sup>3–4</sup>	-1.2
<b>4</b>	Toluene	0.013	10 <sup>4</sup>	-15.0

<sup>a</sup> Calculated in the saturation regime.

<sup>b</sup> This device was fabricated on an HMDS-treated SiO<sub>2</sub> substrate by vacuum deposition.

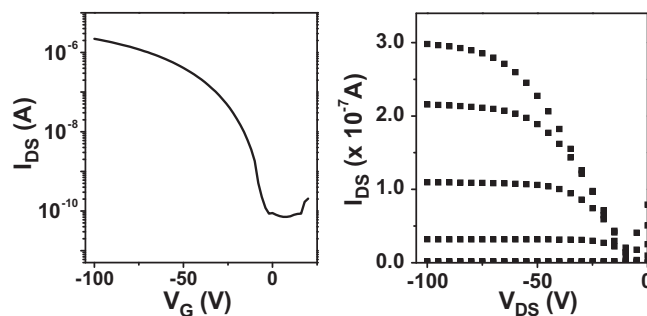


Fig. 8. Transfer and output characteristics of a representative OTFT fabricated with compound **4**. The films were drop-cast from toluene.

was performed in ambient conditions, and the corresponding device characteristics are summarized in Table 3 and Fig. 8 [25].

The devices fabricated with compounds **1–4** all exhibited TFT activity as p-channel semiconductors. In general, enhanced performance was observed: (a) in the **ADT** families versus the **PENs**, and (b) when chlorobenzene was used as the drop-casting solvent. All the compounds employed in this study were sufficiently soluble in common solvents (e.g., toluene, chlorobenzene, and dichlorobenzene) at room temperature. As a preliminary fabrication of the device via solution-process, we prepared for thin films of each compound via drop-casting from the solution. For **PEN** derivatives, the highest carrier mobility values of 0.001 and 0.0004  $\text{cm}^2/\text{V s}$  were observed for films of compounds **1** and **2**, respectively, drop-cast from chlorobenzene. The corresponding  $I_{\text{on}}:I_{\text{off}}$  and  $V_T$  values were  $10^4$  and  $-1$  to  $-7$  V for these **PEN**-based materials. In contrast, **ADT**-based devices fabricated by drop-casting exhibited relatively high mobilities of 0.005  $\text{cm}^2/\text{V s}$  for compound **3** (from chlorobenzene), and 0.013  $\text{cm}^2/\text{V s}$  for compound **4** (from toluene). Similarly to the **PEN** series,  $I_{\text{on}}:I_{\text{off}}$  and  $V_T$  values of  $10^4$  and  $-10$  to  $-15$  V were observed for the **ADT** derivatives. All of the devices were characterized after

two months of storing under nitrogen (without being exposed to light) and did not show any degradation in performance (both mobility and current on/off ratios).

### 3.6. Thin-film microstructure

Film crystallinity and morphology are frequently strongly correlated with OTFT performance. Film morphologies and microstructures for the present new class of materials were studied by optical microscopy and X-ray diffraction for drop-cast thin films. Optical microscopic examination of the drop-cast films revealed pronounced differences in morphology between the **PEN** and **ADT** derivatives (Fig. 9). Polycrystalline platelet-like features were observed for the **ADT**-based films, while relatively fewer crystalline features were observed for drop-cast films of the **PEN** derivatives, which is in accord with the performance of the corresponding TFTs (*vide supra*).

With crystal structure in hand, we could simulate the XRD powder pattern and assign the reflections observed in the film XRD data (Fig. 10). Comparing these data can be useful to analyze the molecular ordering of the compounds. Fig. 10 shows a graphical comparison of experimental and simulated data, with a  $\theta - 2\theta$  scan for a drop-casted film of

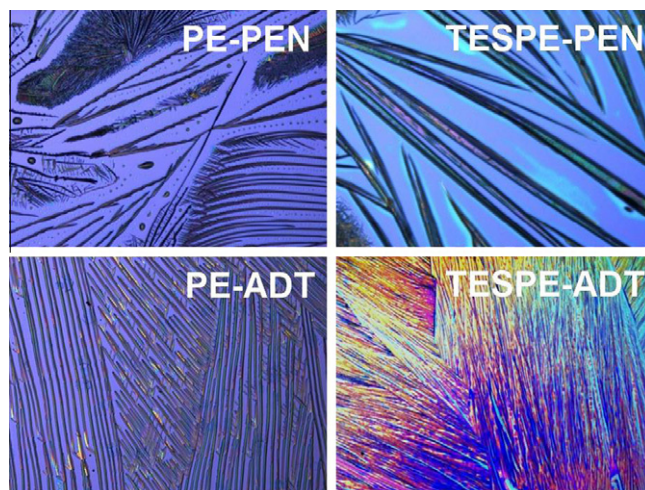
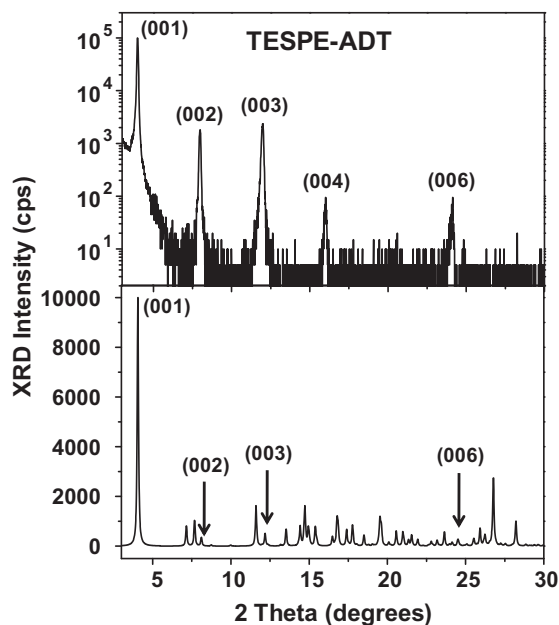


Fig. 9. Optical micrographs of drop-cast films of compounds **1–4**. All images were taken at 50 $\times$  magnification.



**Fig. 10.** Comparison of the  $\theta - 2\theta$  XRD scans of drop-cast films of TESPE-ADT on bare Si/SiO<sub>2</sub> substrates (top) with the simulated powder pattern (bottom).

compound **4** on bare Si/SiO<sub>2</sub> substrate, and a powder pattern generated from the single-crystal data. As shown, (0 0 1) reflection family from (0 0 1) to (0 0 6) was pronounced, indicating predominant ordering of the molecules in *c* direction. For other compounds, the (0 1 1) reflections for compound **1** and (1 2 0) reflections for compound **2** could be assigned, indicating no predominant ordering in the direction of the unit cell axis for both compounds (Fig. S5). For compound **3**, powder pattern did not show (1 0 0) reflections which were present in the film XRD [26].

Overall, the thin film XRD microstructural analysis showed features in agreement with the optical microscopic analysis. Fig. 11 shows representative  $\theta/2\theta$  out-of-plane XRD scans for drop-cast films on bare Si/SiO<sub>2</sub> substrates. As shown, the **ADT** derivatives exhibited more highly textured films having large peak intensities with multiple Bragg reflections. Notably, compound **4** exhibited the highest film texturing with multiple Bragg reflections up to (0 0 6), indicating high film crystallinity and in agreement with the TFT performance (*vide supra*). The estimated *d*-spacing value from the (1 0 0) reflection for compound **4** was 22.2 Å (which corresponds to the length of the *c* axis of the unit cell in the crystal structure), indicating a crystalline polymorph where the majority of the molecules have edge-on orientation on the substrate surface and with the  $\pi$ - $\pi$  stacking direction parallel to the substrate, thereby facilitating in-plane charge transport from source to drain. The diffraction patterns of compounds **1** and **3** showing relatively low carrier mobilities (0.001–0.005 cm<sup>2</sup>/V s) exhibited multiple Bragg reflections (up to three peaks) but with modest peak intensities, and with the latter material evidencing two different phases or growth orientations. Estimated *d*-spacings for these compounds were in the narrow range of 11.6–12.0 Å, probably

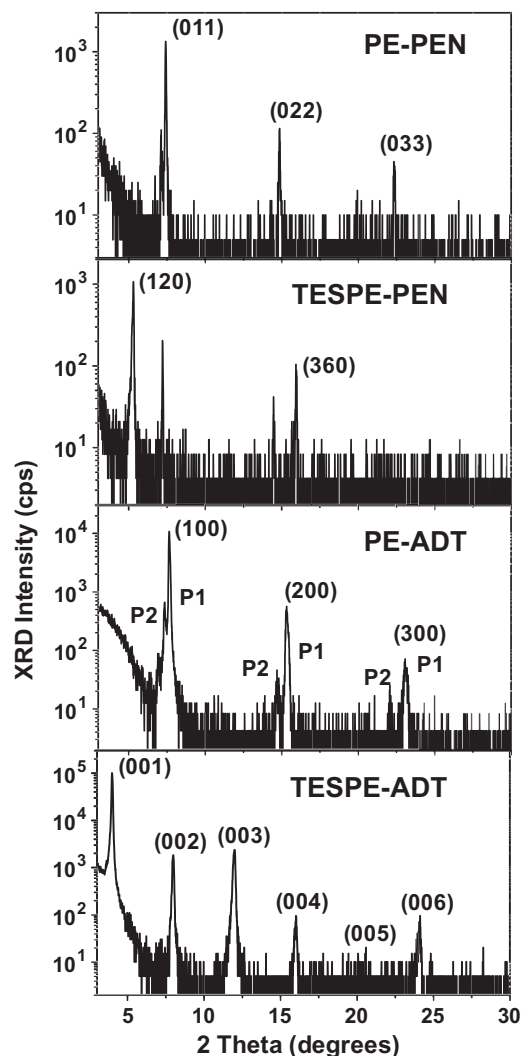


**Fig. 11.** Representative  $\theta - 2\theta$  XRD scans (in logarithmic scale) of drop-cast films of the indicated materials on bare Si/SiO<sub>2</sub> substrates (P1 and P2 indicate two different phases). Peaks are assigned in comparison with the powder pattern generated from the single crystal structures.

indicating similar molecular organization in the films. Compound **2**, with the lowest OTFT performance, exhibited two Bragg reflections having modest peak intensities.

#### 4. Conclusions

In summary, four solution-processable pentacene (**PEN**) and anthradithiophene (**ADT**) derivatives have been synthesized and found to exhibit OTFT p-channel transport. The phenylethynyl substituents were found to be effective in increasing the solubility and environmental stability of the corresponding semiconductors. From the preliminary fabrication of the device via drop-casting, compared to the **PEN** derivatives, the **ADT**-based compounds exhibited higher device performance with respectable carrier mobilities of 0.005–0.013 cm<sup>2</sup>/V s. The magnitudes of the mobilities were strongly correlated with the film

morphology and microstructure. These results provide new information about the structural characteristics of **PEN** and **ADT**-based semiconductors and the attractions of using these cores and substituents for designing more solution-processable OTFT materials. A further complete and detailed device fabrication via other solution-processing methods is underway [22].

### Acknowledgements

We thank the National Science Council, Taiwan, Republic of China (Grant Numbers NSC98-2628-M-008-003, NSC97-2113-M-008-003, and NSC98-2627-E-006-003) and Industrial Technology Research Institute of Taiwan for support. Research at Northwestern was supported by AFOSR (FA9550-08-1-0331) and by the NSF-MRSEC program through the Northwestern Materials Research Center (DMR-0520513).

### Appendix A. Supplementary material

Supplementary data associated with this article can be found, in the online version, at [doi:10.1016/j.orgel.2010.04.029](https://doi.org/10.1016/j.orgel.2010.04.029).

### References

- [1] (a) For recent reviews on this topic, see: A.C. Arias, J.D. MacKenzie, I. McCulloch, J. Rivnay, A. Salleo, *Chem. Rev.* 110 (2010) 3; (b) C.-A. Di, Y. Liu, Y. Yungi, Z. Gui, D. Zhu, *Acc. Chem. Res.* 42 (2009) 1573; (c) M. Chabiny, Y.-L. Loo, *J. Macromol. Sci. Polym. Rev.* 46 (2006) 1; (d) A. Dodabalapur, *Nature* 434 (2005) 151; (e) H. Sirringhaus, *Adv. Mater.* 17 (2005) 2411; (f) A. Facchetti, M.-H. Yoon, T.J. Marks, *Adv. Mater.* 17 (2005) 1705.
- [2] (a) For recent studies, see: X. Gao, C. Di, Y. Hu, X. Yang, H. Fan, F. Zhang, Y. Liu, H. Li, D. Zhu, *J. Am. Chem. Soc.* 132 (2010) ASAP; (b) C. Kim, J.R. Quinn, A. Facchetti, T.J. Marks, *Adv. Mater.* 22 (2010) 342; (c) C. Kim, M.-C. Chen, Y.-J. Chiang, Y.-J. Guo, J. Youn, H. Huang, Y.-J. Liang, Y.-J. Lin, Y.-W. Huang, T.-S. Hu, G.-H. Lee, A. Facchetti, T.J. Marks, *Org. Electron.* (2010) 801; (d) R. Hamilton, M. Heeney, T. Anthopoulos, I. McCulloch, *Org. Electron.* (2010) 393; (e) H. Yan, Z. Chen, Y. Zheng, C.E. Newman, J.R. Quinn, F. Dolz, M. Kastler, A. Facchetti, *Nature* 457 (2009) 679; (f) X. Cheng, Y.-Y. Noh, J. Wang, M. Tello, J. Frisch, R.-P. Blum, A. Vollmer, J.P. Rabe, N. Koch, H. Sirringhaus, *Adv. Funct. Mater.* 19 (2009) 2407; (g) C. Reese, M.E. Roberts, S.R. Parkin, Z. Bao, *Adv. Mater.* 21 (2009) 3678; (h) G.R. Llorente, M.-B. Dufourg-Madec, D.J. Crouch, R.G. Pritchard, S. Ogier, S.G. Yeates, *Chem. Commun.* (2009) 3059; (i) M.-C. Chen, Y.-J. Chiang, C. Kim, Y.-J. Guo, S.-Y. Chen, Y.-J. Liang, Y.-W. Huang, T.-S. Hu, G.-H. Lee, A. Facchetti, T.J. Marks, *Chem. Commun.* (2009) 1846.
- [3] (a) S.K. Park, D.A. Mourey, J.-I. Han, J.E. Anthony, T.N. Jackson, *Org. Electron.* 10 (2009) 486; (b) T.W. Kelly, P.F. Baude, C. Gerlach, D.E. Ender, D. Muires, M.A. Hasse, D.E. Vogel, S.D. Theiss, *Chem. Mater.* 16 (2004) 4413; (c) M.M. Payne, S.R. Parkin, J.E. Anthony, *J. Am. Chem. Soc.* 127 (2005) 4986; (d) C.R. Swartz, S.R. Parkin, J.E. Bullock, J.E. Anthony, A.C. Mayer, G.G. Malliaras, *Org. Lett.* 7 (2005) 3163; (e) D.J. Gundlach, Y.Y. Lin, T.N. Jackson, S.F. Nelson, *Appl. Phys. Lett.* 80 (2002) 2925; (f) H. Meng, M. Bendikov, G. Mitchell, R. Helgeson, F. Wudl, Z. Bao, T. Siegrist, C. Kloc, C.H. Chen, *Adv. Mater.* 15 (2003) 1090; (g) Y. Li, Y. Wu, P. Liu, Z. Prostran, S. Gardner, B.S. Ong, *Chem. Mater.* 19 (2007) 418.
- [4] (a) J.G. Laquindanum, H.E. Katz, A.J. Lovinger, *J. Am. Chem. Soc.* 120 (1998) 664; (b) M.M. Payne, S.A. Odom, S.R. Parkin, J.E. Anthony, *Org. Lett.* 6 (2004) 3325; (c) O.D. Jurchescu, S. Subramanian, R.J. Kline, S.D. Hudson, J.E. Anthony, T.N. Jackson, D.J. Gundlach, *Chem. Mater.* 20 (2008) 6733; (d) M.-C. Chen, C. Kim, S.-Y. Chen, Y.-J. Chiang, M.-C. Chung, A. Facchetti, T.J. Marks, *J. Mater. Chem.* 18 (2008) 1029.
- [5] (a) C.E. Mauldin, K. Puntambekar, A.R. Murphy, F. Liao, V. Subramanian, J.M.J. Frechet, D.M. Delongchamp, D.A. Fischer, M.F. Toney, *Chem. Mater.* 21 (2009) 1927; (b) K. Takimiya, Y. Kunugi, Y. Konda, H. Ebata, Y. Toyoshima, T. Otsubo, *J. Am. Chem. Soc.* 128 (2006) 3044; (c) Y.M. Sun, Y.Q. Ma, Y.Q. Liu, Y.Y. Lin, Z.Y. Wang, Y. Wang, C.A. Di, K. Xiao, X.M. Chen, W.F. Qiu, B. Zhang, G. Yu, W.P. Hu, D. Zhu, *Adv. Funct. Mater.* 16 (2006) 426; (d) K. Xiao, Y. Liu, T. Qi, W. Zhang, F. Wang, J. Gao, W. Qiu, Y. Ma, G. Cui, S. Chen, X. Zhan, G. Yu, J. Qin, W. Hu, D. Zhu, *J. Am. Chem. Soc.* 127 (2005) 13281; (e) X. Zhang, A.P. Cote, A.J. Matzger, *J. Am. Chem. Soc.* 127 (2005) 10502; (f) S. Ando, J. Nishida, H. Tada, Y. Inoue, S. Tokito, Y. Yamashita, *J. Am. Chem. Soc.* 127 (2005) 5336.
- [6] (a) G.S. Tulevski, Q. Miao, A. Afzali, T.O. Graham, C.R. Kagan, C. Nuckolls, *J. Am. Chem. Soc.* 128 (2006) 1788; (b) K.P. Weidkamp, A. Afzali, R.M. Tromp, R.J. Hamers, *J. Am. Chem. Soc.* 126 (2004) 12740.
- [7] (a) J.E. Anthony, J.S. Brooks, D.L. Eaton, S.R. Parkin, *J. Am. Chem. Soc.* 123 (2001) 9482; (b) C.D. Sheraw, T.N. Jackson, D.L. Eaton, J.E. Anthony, *Adv. Mater.* 15 (2003) 2009; (c) C.P. Benard, Z. Geng, M.A. Heuft, K. VanCrey, A.G. Fallis, *J. Org. Chem.* 72 (2007) 7229; (d) D. Lehnher, R. McDonald, R.R. Tykewinski, *Org. Lett.* 10 (2008) 4163.
- [8] (a) Pentacene precursors are soluble derivatives, however, the intrinsic instability of pentacene remains. M.A. Wolak, B.B. Jang, L.C. Palilis, Z.H. Kafafi, *J. Phys. Chem. B* 108 (2004) 5492; (b) A. Maliakal, K. Raghavachari, H. Katz, E. Chandross, T. Siegrist, *Chem. Mater.* 16 (2004) 4980; (c) H. Yamada, Y. Yamashita, M. Kikuchi, H. Watanabe, T. Okujima, H. Uno, T. Ogawa, K. Ohara, N. Ono, *Chem. Eur. J.* 11 (2005) 6212; (d) P. Coppo, S.G. Yeates, *Adv. Mater.* 17 (2005) 3001; (e) A.R. Reddy, M. Bendikov, *Chem. Commun.* (2006) 1179.
- [9] (a) M.M. Payne, S.R. Parkin, J.E. Anthony, C.-C. Kuo, T.N. Jackson, *J. Am. Chem. Soc.* 127 (2005) 4986; (b) S. Subramanian, S.K. Park, S.R. Parkin, V. Podzorov, T.N. Jackson, J.E. Anthony, *J. Am. Chem. Soc.* 130 (2008) 2706.
- [10] R. Schmidt, S. Göttling, D. Leusser, D. Stalke, A. Krause, F. Würthner, *J. Mater. Chem.* 16 (2006) 3708.
- [11] J.E. Anthony, *Chem. Rev.* 106 (2006) 5028.
- [12] D.R. Maulding, B.G. Roberts, *J. Org. Chem.* 34 (1969) 1734.
- [13] Although this 4-triethylsilylphenyl acetylene has been reported in the literature (see ref below) this ligand can be obtained via the Sonogashira coupling in a simple procedure with good yield. C. Eaborn, A.R. Thompson, D.R.M. Walton, *J. Chem. Soc. C. Org.* 15 (1967) 1364.
- [14] S.M. Sze, *Physics of Semiconductor Devices*, second ed., John Wiley & Sons, USA, 1981.
- [15] Since the concentration of the solution has a strong influence on the rate of decomposition, a very dilute solution ( $\sim 4.0 \times 10^{-5}$  M) was used.
- [16] Alkynyl substitution lowers the LUMO energy for pentacene derivatives as compared to that of pentacene, which has been known to hinder photooxidation. M. Akhtaruzzaman, N. Kamata, J. Nishida, S. Ando, H. Tada, M. Tomura, Y. Yamashita, *Chem. Commun.* (2005) 3183, and Ref. [3a].
- [17] Because Pen is not sufficiently soluble, the DPV was performed at high temperature. There was no indication of thermal decomposition under this condition (under  $N_2$ ).
- [18] Measured with a Pt working electrode in an *o*-dichlorobenzene solution using 0.1 mol dm<sup>-3</sup> Bu<sub>4</sub>NPF<sub>6</sub> as the supporting electrolyte. N. Jun-ichi Nishida, D. Kumaki, S. Tokito, Y. Yamashita, *J. Am. Chem. Soc.* 128 (2006) 9598.
- [19] Similar trends were reported in: J. Wang, K. Liu, Y.-Y. Liu, C.-L. Song, Z.-F. Shi, J.-B. Peng, H.-L. Zhang, X.-P. Cao, *Org. Lett.* 11 (2009) 2563.
- [20] The planar angle ( $\sim 8.1^\circ$ ) and interweaving angle ( $82^\circ$ ) were smaller for BBPE-Pen with an interplanar core distance of 3.44 Å. In

- comparison, both the interplanar distances of compound **1** (3.40 Å) and **3** (3.34 Å) were shorter than BBPE-Pen.
- [21] J.E. Anthony, D.L. Eaton, S.R. Parkin, *Org. Lett.* **4** (2002) 15.
- [22] Improved TFT performance for compound **4** was achieved by device fabrication via spin-coating.
- [23] Standard deviations for 5 devices are typically <20%.
- [24] All the compounds were fabricated via vacuum deposition on bare Si/SiO<sub>2</sub> and HMDS-treated substrates at various temperatures. But only one compound (compound **3**) exhibited good device performance. The other compounds are inactive or exhibit very low performance (mobility <10<sup>-6</sup> cm<sup>2</sup>/V s).
- [25] All the available data for all compounds are in the Supporting Information (Tables S1–S2 and Figs. S1–S4).
- [26] Except compound **4**, the X-ray diffraction pattern of the semiconductor films did not match the simulated powder pattern. This is likely due to polymorph formation (which is clearly shown in compound **3**).